



# 1 Wall loss of semi-volatile organic compounds in a Teflon bag chamber 2 for the temperature range of 262-298 K

3 Longkun He<sup>1</sup>, Wenli Liu<sup>2</sup>, Yatai Li<sup>1,3</sup>, Jixuan Wang<sup>1</sup>, Mikinori Kuwata<sup>2</sup>, Yingjun Liu<sup>1</sup>

4 <sup>1</sup>State Key Joint Laboratory of Environmental Simulation and Pollution Control, College of Environmental Sciences and  
5 Engineering, Peking University, Beijing, 100871, China

6 <sup>2</sup>Department of Atmospheric and Oceanic Sciences and Laboratory for Climate and Ocean-Atmosphere Studies, School of  
7 Physics, Peking University, Beijing 100871, China

8 <sup>3</sup>Now at College of Public Health, Zhengzhou University, Zhengzhou, 450001, China

9 Correspondence to: Mikinori Kuwata ([kuwata@pku.edu.cn](mailto:kuwata@pku.edu.cn)), Yingjun Liu ([yingjun.liu@pku.edu.cn](mailto:yingjun.liu@pku.edu.cn))

10

11 **Abstract.** Teflon bag chambers have long been used for investigating atmospheric chemical processes, including secondary  
12 organic aerosol formation. Wall-loss process of gas-phase species in Teflon bag chambers has typically been investigated at  
13 around room temperature. Recent laboratory studies started employing Teflon bag chambers at sub-273 K conditions for  
14 simulating wintertime and upper tropospheric environments. However, temperature dependence in vapor wall-loss processes  
15 of semi-volatile organic compounds (SVOCs) in a Teflon bag chamber has not well been investigated. In this study, we  
16 experimentally investigated wall-loss process of C<sub>14</sub>-C<sub>19</sub> *n*-alkanes in a 1 m<sup>3</sup> Teflon bag for the temperature range of 262 to  
17 298 K. Enhanced wall losses of the tested *n*-alkanes were observed following the decrease in temperature. For instance, 65%  
18 of C<sub>14</sub> *n*-alkane was lost to the wall 15 hours after injection at room temperature, while the corresponding value was 95% at  
19 262 K. The experimental data were analyzed using the two-layer kinetic model, which considers both absorption of gas phase  
20 species to the surface layer of Teflon wall and diffusion to the inner layer. The experimental data demonstrated that absorption  
21 of gas phase species by the surface layer enhanced at lower temperature. The temperature dependence in absorption was well  
22 accounted using the equilibrium dissolution model of organic compounds to the Teflon surface by considering reduced  
23 saturation vapor pressure at lower temperature. On the contrary, diffusion process of *n*-alkanes from the surface to inner layer  
24 slowed down at reduced temperature. Hence the relative importance of the surface and inner layers on wall-loss process  
25 changes with temperature. Mechanistic studies on these processes will need to be conducted in the future to quantitatively  
26 predict the influence of temperature-dependent wall-loss processes of SVOCs on laboratory experimental results.



## 27 1 Introduction

28 The environmental chamber is one of the most widely-used laboratory systems for studying chemical processes in  
29 the atmosphere, including formation of secondary organic aerosol (SOA) (Clark et al., 2016; Nakao et al., 2011; Ng et al.,  
30 2007; Song et al., 2005). The environmental chambers are typically made of Teflon films or stainless steel (Cocker et al., 2001;  
31 Bunz et al., 1996; Voigtlaender et al., 2012). Existence of walls in the environmental chambers induces losses of both vapors  
32 and particles due to their deposition on wall surfaces (McMurry and Grosjean, 1985; Krechmer et al., 2020). Wall loss of gas-  
33 phase organic compounds in the environmental chambers can lead to underestimation of SOA mass yields. For instance,  
34 injection of seed particles into Teflon bag has been shown to increase SOA yields by a few times due to the reduced relative  
35 importance of the chamber wall as a condensation sink in the system (Kroll et al., 2007; Zhang et al., 2014).

36 Vapor wall loss in Teflon bag chambers, especially that for semi-volatile organic compounds (SVOCs), has been  
37 intensively investigated in the last decade (Matsunaga and Ziemann, 2010; Yeh and Ziemann, 2014; Yeh and Ziemann, 2015;  
38 Zhang et al., 2015; Krechmer et al., 2016; Huang et al., 2018b; Pratap et al., 2020; Yu et al., 2022). For instance, Matsunaga  
39 and Ziemann (2010) studied wall-loss process of alkanes, alkenes, alcohols, and ketones. These previous wall-loss experiments  
40 were dominantly conducted at around room temperature (293~303 K), as most of the chamber studies employed the  
41 corresponding temperature range (Hidy, 2019). The experimental results were often modeled by assuming equilibrium  
42 dissolution of the organic compounds into the Teflon film. A more recent study separately considered the surface and inner  
43 layer of the Teflon film for explaining the loss process more quantitatively (Huang et al., 2018b).

44 Recently, a growing number of environmental chamber experiments have been conducted at low temperatures to  
45 simulate wintertime/upper tropospheric conditions in laboratory (Huang et al., 2018a; Pratap et al., 2019; Quelever et al., 2019;  
46 Simon et al., 2020; Wang et al., 2022). For instance, some SOA formation experiments have been conducted for the  
47 temperature range down to 223 K using stainless steel chambers such as the Aerosol Interaction and Dynamics in the  
48 Atmosphere (AIDA) and Cosmics Leaving Outdoor Droplets (CLOUD) chambers (Huang et al., 2018a; Simon et al., 2020).  
49 Teflon bag chambers have also been employed for the temperature range down to 258 K (Kristensen et al., 2017; Deng et al.,  
50 2021). These studies demonstrate that temperature is an important parameter determining both mass yields and chemical  
51 composition of SOA. Vapor wall loss of SVOCs in the environmental chambers for the corresponding temperature range needs  
52 to be understood for better interpreting these experimental data in a quantitative way. So far only one group attempted to  
53 investigate vapor wall loss below room temperature, by measuring the size evolution of levoglucosan particles injected into a  
54 Teflon chamber (Pratap et al., 2020). However, the experimental results were confounded by slow evaporation of levoglucosan  
55 from particles at low temperatures.

56 This study investigated vapor wall loss of C<sub>14</sub>-C<sub>19</sub> *n*-alkanes in a Teflon chamber for the temperature range of 262 to  
57 298 K by monitoring the evolution of their gas-phase concentrations following a pulse release. The experimental results were



58 analyzed using the two-layer kinetic model, which considers partitioning of gas phase SVOCs to the surface layer, as well as  
59 further diffusion to the inner layer. Temperature effects on the two processes were evaluated separately.

## 60 2 Experimental

### 61 2.1 Teflon chamber experiments

62 Figure 1 shows the experimental setup. The experiment was conducted using a fluorinated ethylene propylene (FEP)  
63 bag with the volume of  $1 \text{ m}^3$ . The thickness of the FEP film for the bag was  $75 \text{ }\mu\text{m}$ . The dimension of the bag was  $260 \text{ cm} \times$   
64  $55 \text{ cm} \times 70 \text{ cm}$ . The chamber volume was experimentally validated by employing  $\text{CO}_2$  as a tracer (Figure S1). The bag was  
65 newly purchased for the experiment, meaning that it was employed for no other experiments. The bag was installed in a chest  
66 freezer (Type 2288, Nixue Inc.), which was equipped with an additional internal thermal insulation layer. Two fans were  
67 installed in the freezer to promote the mixing of the air. The temperature of the freezer was measured at 3 points using  
68 temperature sensors (Figure 1). Temporal variation of temperature was  $\pm 0.5 \text{ K}$  at  $262 \text{ K}$ .

69 Throughout the experiments, purified air was employed. The purified air was produced using a zero air generator  
70 (Model 747–30, AADCO Instruments, Inc.) and further purified using a hydrocarbon trap (BHT-2, Agilent Technologies, Inc.).  
71 Hydrocarbon concentration in the purified air was less than  $5 \text{ ppbv}$ . Relative humidity (RH) was less than  $0.1\%$ .

72 Solutions containing  $\text{C}_{14}$  -  $\text{C}_{19}$  *n*-alkanes (Konoscience Inc.,  $> 98\%$ ) were prepared and injected into the chamber.  
73 Hexane (Fisher Chemical Co., HPLC grade) was employed as the solvent. The purities and saturation vapor pressures of all  
74 chemicals are given in Table S1. The solutions were injected to the chamber using a syringe pump (Fusion 200 Touch, Chemyx  
75 Inc.) and a nebulizer (TR-30-A1, Meinhard Inc.) through polytetrafluoroethylene (PTFE) tubing, as shown in Figure 1. The  
76 use of nebulizer expedited the evaporation of the solution.

77 Eight sets of wall-loss experiments were conducted in the temperature range of  $262$  to  $298 \text{ K}$ . Prior to each experiment,  
78 the chamber was continuously flushed using purified air, until the concentration of investigated *n*-alkanes dropped to the  
79 background level. To start an experiment, the chamber was switched to batch mode and the solution was injected to the  
80 chamber at room temperature. The injection lasted for 13 mins, with a liquid flow rate of  $100 \text{ }\mu\text{L min}^{-1}$ . The air flow rate of  
81 the nebulizer was  $0.7 \text{ L min}^{-1}$ . The resulting initial concentrations ( $C_0$ ) of individual *n*-alkanes in the chamber ranged from  $4$   
82 to  $50 \text{ }\mu\text{g m}^{-3}$  assuming no wall loss. The solution used for low-temperature experiments ( $< 278 \text{ K}$ ) did not contain  $\text{C}_{18}$  and  $\text{C}_{19}$   
83 *n*-alkanes to avoid formation of particles. For experiments below room temperature, the cooling system of the freezer was  
84 turned on one hour after the completion of the injection. The operation procedure was employed to avoid homogeneous  
85 nucleation and subsequent condensational growth of aerosol particles. Measurements using an optical particle counter (11-D,  
86 GRIMM Aerosol Technik Ainring, Germany) experimentally confirmed negligible abundance of aerosol particles in the  
87 chamber ( $< 0.5 \text{ }\mu\text{g m}^{-3}$ ). It took  $\sim 3$  hours for the temperature in the freezer to drop to a stable level after injection (Figure S2).



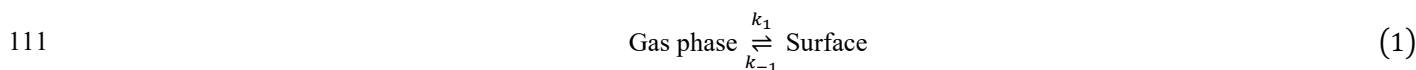
88 Although the air in the bag leaked out during experiments due to compression of the bag by its own weight, absence of intrusion  
89 of room air to the bag was confirmed by observing no changes in contaminant signals (Table S2).

90 Concentrations of SVOCs in the chamber were quantified using the semi-volatile thermal desorption aerosol gas  
91 chromatograph (SV-TAG, Aerodyne Research Inc. & Aerosol Dynamic Inc., USA) (Zhao et al., 2013). The gas  
92 chromatography-mass spectrometer (GC-MS) (7890B, Agilent Technologies, Inc.) was employed for the system. Detailed  
93 descriptions of the SV-TAG operation and performance tests were presented in our previous papers (Li et al., 2022a; Li et al.,  
94 2022b). Herein, chamber air was sampled through ~1 m long perfluoroalkoxy alkane (PFA) tubing (1/4 inch in diameter). Prior  
95 to sampling, the chamber air passed through the PFA tubing at 0.5 L min<sup>-1</sup> for at least 20 min for passivating the tubing wall  
96 (Matsunaga and Ziemann, 2010). Samples were periodically collected for 5 min at 4 L min<sup>-1</sup> for each time at 1-15 hours after  
97 injection. As the absence of particles was confirmed, only gas-phase SVOCs were sampled by the SV-TAG. The instrument  
98 response to *n*-alkanes was calibrated with standards before and after each experiment (Figure S3), utilizing the in-situ automatic  
99 injection system (Isaacman et al., 2011). The gas-phase concentrations of SVOCs were calculated from the measured quantity  
100 of SVOCs and sampled air volume.

## 101 2.2 Kinetic model

102 Herein we used a unified vapor wall-loss transport model developed by Huang et al. (2018b) to fit the experimental  
103 data. Figure 2 shows the concept of the model. Briefly, SVOCs partition between the gas phase and the surface of the FEP  
104 film. Subsequently, the absorbed SVOCs may diffuse to the inner layer of the film. As the thickness of the FEP film (75 μm)  
105 is a couple of orders larger than that of the surface layer (~ 5 nm) (Huang et al., 2018b), the inner layer is assumed as an  
106 infinite sink. As a result, the diffusion process of SVOCs from the inner layer to the film surface is ignored. A list of all the  
107 parameters is provided in Nomenclature. The governing equations without and with considering diffusion to the inner layer  
108 are presented below, respectively.

109 (1) Without considering the diffusion process in the inner layer, the wall loss process is solely controlled by  
110 partitioning of SVOCs between the gas phase and surface layer and can be described as follows



112 where  $k_1$  and  $k_{-1}$  are forward and backward rate constants in the process. The corresponding first-order kinetic equations are

$$113 \begin{aligned} \frac{dC_{gas}}{dt} &= -k_1 C_{gas} + k_{-1} C_{surface} \\ \frac{dC_{surface}}{dt} &= k_1 C_{gas} - k_{-1} C_{surface} \end{aligned} \quad (2)$$



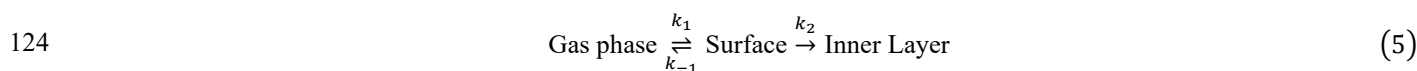
114 where  $C_{gas}$  and  $C_{surface}$  are the SVOC concentrations in gas phase and on wall surface, respectively. It should be noted that  
115  $C_{surface}$  was defined as the total mass of SVOC that was divided by the chamber volume, following previous studies  
116 (Matsunaga and Ziemann, 2010; Yeh and Ziemann, 2014; Yeh and Ziemann, 2015). This model has been commonly used to  
117 interpret the experimental data of vapor wall loss in previous studies (Matsunaga and Ziemann, 2010; Yeh and Ziemann,  
118 2014; Yeh and Ziemann, 2015; Zhang et al., 2015).

119 The gas-surface equilibrium time scale  $\tau_{surface}$  and equilibrium constant  $K_{eq}$  can be obtained by

120 
$$\tau_{surface} = \frac{1}{k_1 + k_{-1}} \quad (3)$$

121 
$$K_{eq} = \frac{k_1}{k_{-1}} = \left[ \frac{C_{surface}}{C_{gas}} \right]_{eq} \quad (4)$$

122 (2) Considering the diffusion process in the inner layer, the whole vapor wall loss process can be formulated as  
123 follows



125 where  $k_2$  is the first-order loss rate constant in the diffusion process. Correspondingly, the kinetic processes for  $C_{gas}$  and  
126  $C_{surface}$  can be described by the following equations

127 
$$\begin{aligned} \frac{dC_{gas}}{dt} &= -k_1 C_{gas} + k_{-1} C_{surface} \\ \frac{dC_{surface}}{dt} &= k_1 C_{gas} - k_{-1} C_{surface} - k_2 C_{surface} \end{aligned} \quad (6)$$

128 The diffusion process has the first-order decay time scale  $\tau_{inner}$  of  $\tau_{inner} = \frac{1}{k_2}$ . If  $k_2 \ll k_1 + k_{-1}$  (i.e.,  $\tau_{inner} \gg \tau_{surface}$ ),  
129 gas-surface partitioning occurs much faster than the diffusion process to the inner layer. In this case, the loss rate of SVOC  
130 from the gas phase can asymptotically be represented as

131 
$$\frac{dC_{gas}}{C_{gas} dt} \approx -\frac{K_{eq}}{1 + K_{eq}} k_2 \quad (7)$$

132 The data analysis and model fitting were conducted using Wolfram Mathematica 13.1. The controlling factors of  
133 individual parameters in the above equations were previously discussed by Huang et al. (2018b).



## 134 3 Results and discussion

### 135 3.1 Wall loss of *n*-alkanes at room temperature

136 An example of temporal profile for  $C_{14}$ - $C_{19}$  *n*-alkanes during the experiment at 298 K is shown in Figure 3. The figure  
137 demonstrates the temporal change of  $C_{gas}/C_0$ , where  $C_0$  indicates the initial concentration of *n*-alkanes. The values of  $C_{gas}/C_0$   
138 for each *n*-alkane exhibited similar patterns. During the first one hour following the injection,  $C_{gas}/C_0$  exponentially decreased.  
139 After that, gradual decreases in  $C_{gas}/C_0$  were observed. For example, the decline in gas fraction for  $C_{14}$  *n*-alkane during the  
140 first hour accounted for 71% of the total change in  $C_{gas}/C_0$  over the whole experimental period of 15 hours. The values of  
141  $C_{gas}/C_0$  decreased with the increase in carbon number, indicating enhanced wall loss. The values of  $C_{gas}/C_0$  at 15 hours after  
142 injection were 0.32, 0.25, 0.16, 0.097, 0.069, and 0.037 for  $C_{14}$  -  $C_{19}$  *n*-alkanes, respectively.

143 The experimental result can be well fitted using the two-layer model, but the fits deteriorate in the case that diffusion  
144 in the inner layer is neglected (Figure 3). The optimized parameter sets are shown in Table S3. Mass fractions of injected  
145 chemical species in the gas, surface, and inner layer phases that were estimated using the model are shown in Figure S4. In the  
146 case of the most volatile compound ( $C_{14}$  *n*-alkane), the maximum mass fraction in the surface phase occurred at 2 hours after  
147 injection. Subsequently, the mass fractions for the compound in both gas phase and surface layer gradually decreased. During  
148 this period, the ratio of the mass in the surface layer to that in the gas phase stabilized at 1.33. The mass fraction of the  
149 compound in the inner layer steadily increased, reaching 0.22 at 15 hours after injection.

150 In the case of the least volatile compound ( $C_{19}$  *n*-alkane), the mass fraction in the surface layer reached the maximum  
151 (~76%) approximately 1 hour after injection, accounting for the rapid decrease in the observed concentration in the gas phase.  
152 Subsequently, mass fractions of the compound in the gas phase and in the surface layer decreased in proportion, maintaining  
153 a constant ratio of the two (Figure S4). The mass fraction of the compound in the inner layer kept increasing during the  
154 experiment. At 15 hours after injection, 87% of the compound existed in the inner layer.

155 The time scale for *n*-alkanes to reach partitioning equilibrium between the gas and surface phases is estimated to be  
156 12 ~ 35 mins, consistent with literature data. For example, Matsunaga and Ziemann (2010) reported that the corresponding  
157 time scale for  $C_8$  -  $C_{16}$  alkanes was  $60 \pm 20$  mins. The corresponding value for oxygenated organic compounds was reported  
158 as  $26 \pm 23$  mins (Yeh and Ziemann, 2015).

159 Our result for the mass transfer of SVOCs to the inner layer can also be compared with a previous study. The rates  
160 for the decrease in  $C_{gas}/C_0$  for  $C_{14}$ - $C_{19}$  *n*-alkanes were 0.6–1.3% hour<sup>-1</sup> after the partitioning between gas phase and surface  
161 layer reached equilibrium (*i.e.*, 3 ~ 15 hours). Yeh and Ziemann (2015) reported the corresponding value for 2-ketones as  
162 approximately 1% hour<sup>-1</sup> for the time scale of 7 hours. They suggested that the value is close to the theoretical value for the  
163 Fickian diffusion loss rate (~0.5 % hour<sup>-1</sup>).



### 164 3.2 Temperature dependence of wall loss of *n*-alkanes

165 Figure 4a summarizes the values of  $C_{gas}/C_0$  for all experiments at 3 hours after injection. The data for this sampling  
166 time was selected, as the loss of gas phase species by partitioning to the surface layer accounted for the dominant portion of  
167 the decline in the gas phase concentration. It should be noted that fitting the experimental data using the two-layer model was  
168 challenging for the low-temperature experiments, as the chamber was cooled after the injection of *n*-alkanes. Potential  
169 uncertainties associated with the employment of the data at 3 hours after injection as a proxy for gas-surface partitioning are  
170 summarized in Text S1.

171 Generally,  $C_{gas}/C_0$  was lower for less volatile compounds and at lower temperature, suggesting enhanced partitioning  
172 of *n*-alkanes to the chamber wall. The data for the room temperature ( $C_{gas}/C_0 = 0.47, 0.45, 0.34, 0.24, 0.17,$  and  $0.091$  for  $C_{14},$   
173  $C_{15}, C_{16}, C_{17}, C_{18},$  and  $C_{19}$  *n*-alkanes) were smaller than that have been reported by a previous study. Namely, Matsunaga and  
174 Ziemann (2010) quantified the corresponding values for equilibration between the gas and surface phases for  $C_{14}$ - $C_{16}$  *n*-alkanes  
175 as  $\sim 80 - 90\%$ . The enhanced partitioning to the surface layer in our study is likely due to that the chamber we used is smaller  
176 ( $1 \text{ m}^3$  versus  $5.9 \text{ m}^3$ ).

177 Figure 4b shows the values of  $C_{gas}/C_0$  as a function of temperature at 15 hours after injection. In all experiments, the  
178 values of  $C_{gas}/C_0$  at 15 hours after injection were consistently lower than those for 3 hours. For instance,  $C_{gas}/C_0$  for  $C_{14}$  *n*-  
179 alkane at 262 K decreased from 0.15 (3 hours) to 0.06 (15 hours). As discussed in the case of the experiment at 298 K, the  
180 result suggests that diffusional loss in the inner layer of the chamber wall occurred for the whole temperature range.

### 181 3.3 Temperature dependence of partitioning between gas phase and wall surface

182 The temperature dependence in the data summarized in Figure 4a can be understood by considering changes in  
183 partitioning between the gas phase and surface layer. Matsunaga and Ziemann (2010) introduced the following equation for  
184 relating  $C_{surface}/C_{gas}$  and temperature based on the equilibrium dissolution model:

$$185 \left[ \frac{C_{surface}}{C_{gas}} \right]_{eq} = K_{eq} = \frac{C_{FEP\_surface} RT}{M_{wall} \gamma_{FEP\_surface} P_s(T)} \quad (8)$$

186 where  $C_{FEP\_surface}$  is the equivalent organic mass concentration of the FEP chamber surface wall,  $M_{wall}$  is the average  
187 molecular mass of the FEP,  $\gamma_{FEP\_surface}$  is the activity coefficient of the organic compound in the Teflon surface,  $R$  is the gas  
188 constant, and  $T$  is temperature.  $P_s(T)$  is the saturation vapor pressure of the compound at temperature  $T$ . To use Equation (8)  
189  $P_s(T)$  was calculated by the EVAPORATION group contribution method (Compernelle et al., 2011). Comparison between  
190 the EVAPORATION method with other approaches for estimating  $P_s(T)$  is available in Figure S5. The value of



191  $[C_{surface}/C_{gas}]_{eq}$  was approximated using  $1/[C_{gas}/C_0]_{at\ 3\ hours} - 1$  by assuming that diffusion of *n*-alkanes to the inner layer  
192 was still a minor loss process within 3 hours. Among the terms for the right-hand-side of equation (8),  $RT/P_s(T)$  can be  
193 calculated from the experimental conditions. The equation suggests that  $[C_{surface}/C_{gas}]_{eq}$  and  $RT/P_s(T)$  may linearly  
194 correlate with the slope of  $C_{FEP\_surface}/(M_{wall}\gamma_{FEP\_surface})$ .

195 Figure 5 shows the correlations between  $C_{surface}/C_{gas}$  and  $RT/P_s(T)$  for individual compounds. For all the tested  
196 compounds, these two parameters correlated well, even though  $C_{surface}/C_{gas}$  increased by more than one order of magnitude  
197 when the chamber was cooled down. The result suggests that equation (8) can be applied to a wide range of temperatures  
198 without considering the temperature dependence of  $C_{FEP\_surface}/(M_{wall}\gamma_{FEP\_surface})$  to account for partitioning of a chemical  
199 species to the surface layer. In other word,  $\gamma_{FEP\_surface}$  can be practically treated as a constant for the investigated temperature  
200 range, given  $C_{FEP\_surface}$  and  $M_{wall}$  are independent of temperature. This implication is consistent with previous findings that  
201 the activity coefficients of organic compounds in polymers only change slightly with temperature. For instance, Kontogeorgis  
202 et al. (1993) compared the experimental and modelled values of activity coefficients for hydrocarbons in a few polymers such  
203 as low-density polyethylene. The values of activity coefficients change by 10~20% for a temperature change of 100 K.

204 Values of  $\gamma_{FEP\_surface}$  for *n*-alkanes can be estimated from Figure 5. Based on equation (8), the fitted slopes  
205 correspond to  $C_{FEP\_surface}/(M_{wall}\gamma_{FEP\_surface})$ . For a specific chamber design, compound-independent  $C_{FEP\_surface}$  can be  
206 estimated by the density of FEP film (2150 kg m<sup>-3</sup>) and the thickness of surface layer (~ 5 nm) (Huang et al., 2018b). For the  
207 chamber in this experiment,  $C_{FEP\_surface} = 78.2\text{ mg m}^{-3}$ . For estimating compound-dependent  $\gamma_{FEP\_surface}$ , previous studies  
208 assumed  $M_{wall} = 200\text{ g mol}^{-1}$  (Huang et al., 2018b; Matsunaga and Ziemann, 2010). The same approximations were employed  
209 in the present study.

210 Figure 6 plots the retrieved values of  $\gamma_{FEP\_surface}$  for *n*-alkanes against  $P_s(298\text{ K})$  for *n*-alkanes. The figure also  
211 shows the corresponding parameters obtained from previous experimental studies (Matsunaga and Ziemann, 2010; Yeh and  
212 Ziemann, 2014; Yeh and Ziemann, 2015; Krechmer et al., 2016). Regardless of differences in types of chemicals and chambers,  
213 the experimentally estimated values of  $\gamma_{FEP\_surface}$  and  $P_s(298\text{ K})$  correlate in logarithmic axes. The relationship followed  
214 the equation of  $\ln(\gamma_{FEP\_surface}) = 0.40 - 0.61\ln(P_s(298\text{ K}))$ .

### 215 3.4 Characterization of diffusion from the Teflon surface to inner layer

216 Values of  $k_2$  were estimated using equation (7), since values of  $\tau_{inner}$  are at least 18 times larger than those of  
217  $\tau_{surface}$  (Table S3). The values of  $C_{gas}/C_0$  at 3 hours after injection were employed to calculate  $K_{eq}$  as discussed earlier.  
218 The experimental data for 9, 12, and 15 hours after injection was employed for obtaining  $k_2$ .



219 Figure 7 plots the estimated values of  $k_2$  against  $P_s(T)$  for all compounds in all experiments. The values of  $k_2$  and  
220  $P_s(T)$  positively correlate. As a comparison point, a previous study reported positive correlations for (1) the diffusivity of  
221 organic compounds in FEP film and saturation concentration, and (2)  $k_2$  and diffusivity (Huang et al., 2018b). Our current  
222 result is qualitatively similar to the previous study, though temperature was maintained as a constant in the previous study.  
223 The decrease in  $k_2$  at lower temperature could be induced by reduced viscosity in the inner layer or weakened thermal motion  
224 of *n*-alkane molecules. Further research, that incorporates changes in FEP film properties with temperature would be needed  
225 in the future for quantitatively interpreting the data.

#### 226 4 Conclusions

227 The present study investigated the wall loss process of C<sub>14</sub>-C<sub>19</sub> *n*-alkanes to the wall of a 1 m<sup>3</sup> chamber bag, which was  
228 composed of the FEP film. The temperature of the chamber was controlled for the range of 262 to 298 K. Decay in gas-phase  
229 concentrations of the *n*-alkanes was quantified using the SV-TAG for 15 hours following injection. The temporal variations in  
230 the *n*-alkane concentrations suggested two types of loss processes. The first process was characterized by rapid exponential  
231 decay in the first few hours. Subsequently, slow first-order decreases in the *n*-alkane concentrations were identified until the  
232 end of the experiment. Enhanced wall loss was observed at lower temperatures for all compounds.

233 The experimental data were well fitted using the two-layer kinetic model, which considers partitioning of gas-phase  
234 species to the surface layer of the chamber film and further diffusion to the inner layer. The analysis suggests that when the  
235 Teflon bag chamber is operated at low temperatures, partitioning of gas phase species to the chamber wall surface is enhanced,  
236 whereas the permeation of the chemical compounds to the inner layer is suppressed. The temperature effect on gas-surface  
237 partitioning overweighs that on diffusion into the inner layer for *n*-alkanes, leading to an overall enhanced wall loss at lower  
238 temperature.

239 The quasi-equilibrium partitioning of *n*-alkanes between the gas phase and surface layer was interpreted by considering  
240 the dissolution process of the species into the surface layer. Values of  $C_{surface}/C_{gas}$  at quasi-equilibrium are proportional to  
241  $RT/P_s(T)$  for individual compounds. The result suggests that decreased saturation vapor pressure is the major driving force  
242 for enhanced partitioning to the surface layer at low temperatures for all investigated compounds, while their activity  
243 coefficients can be practically treated as constants for the investigated temperature range. The relationship can be potentially  
244 employed for predicting changes in wall loss of SVOCs as a function of temperature, after further verification employing other  
245 types of organic compounds.

246 In the future, the underlying mechanisms of the present findings will need to be sought for a better understanding of the  
247 chamber wall loss of SVOCs. The present study focused on *n*-alkanes. In the case of chamber experiments for SOA formation,  
248 wall loss processes of oxygenated chemical species would be more important. Thus, a temperature-dependent wall loss study



249 for oxygenated chemical species will still need to be conducted for interpreting SOA chamber experiments under a wide range  
250 of temperatures.

#### 251 **Data Availability**

252 Data will be made available on request.

#### 253 **Author contribution**

254 **Longkun He:** Conceptualization, Methodology, Experiment, Data curation, Formal analysis, Writing – original draft. **Wenli**  
255 **Liu:** Methodology, Experiment, Writing – review & editing. **Yatai Li:** Methodology, Writing – review & editing. **Jixuan**  
256 **Wang:** Experiment, Writing – review & editing. **Mikinori Kuwata:** Conceptualization, Methodology, Project administration,  
257 Funding acquisition, Formal analysis, Writing – review & editing, Supervision. **Yingjun Liu:** Conceptualization,  
258 Methodology, Project administration, Funding acquisition, Formal analysis, Writing – review & editing, Supervision.

#### 259 **Competing interests**

260 The authors declare that they have no conflict of interest.

#### 261 **Acknowledgements**

262 We thank Dr. Ying Zhou for assisting to improve figure quality. This research was supported by the National Natural  
263 Science Foundation of China (92044303, 42175121, and 42150610485).



## 264 Reference

- 265 Bunz, H., Möhler, O., Naumann, K., Saathoff, H., Schöck, W., and Schurath, U.: The novel aerosol chamber facility AIDA:  
266 status and first results, Proc. 7th European Symposium on the Physico-Chemical Behaviour of Atmospheric Pollutants,  
267 1996.
- 268 Clark, C. H., Kacarab, M., Nakao, S., Asa-Awuku, A., Sato, K., and Cocker, D. R., III: Temperature Effects on Secondary  
269 Organic Aerosol (SOA) from the Dark Ozonolysis and Photo-Oxidation of Isoprene, Environ. Sci. Technol., 50, 5564-  
270 5571, <https://doi.org/10.1021/acs.est.5b05524>, 2016.
- 271 Cocker, D. R., Flagan, R. C., and Seinfeld, J. H.: State-of-the-art chamber facility for studying atmospheric aerosol chemistry,  
272 Environ. Sci. Technol., 35, 2594-2601, <https://doi.org/10.1021/es0019169>, 2001.
- 273 Compernelle, S., Ceulemans, K., and Muller, J. F.: EVAPORATION: a new vapour pressure estimation method for organic  
274 molecules including non-additivity and intramolecular interactions, Atmos. Chem. Phys., 11, 9431-9450,  
275 <https://doi.org/10.5194/acp-11-9431-2011>, 2011.
- 276 Deng, Y. G., Inomata, S., Sato, K., Ramasamy, S., Morino, Y., Enami, S., and Tanimoto, H.: Temperature and acidity  
277 dependence of secondary organic aerosol formation from alpha-pinene ozonolysis with a compact chamber system,  
278 Atmos. Chem. Phys., 21, 5983-6003, <https://doi.org/10.5194/acp-21-5983-2021>, 2021.
- 279 Hidy, G. M.: Atmospheric Chemistry in a Box or a Bag, Atmosphere, 10, <https://doi.org/10.3390/atmos10070401>, 2019.
- 280 Huang, W., Saathoff, H., Pajunoja, A., Shen, X. L., Naumann, K. H., Wagner, R., Virtanen, A., Leisner, T., and Mohr, C.:  
281 alpha-Pinene secondary organic aerosol at low temperature: chemical composition and implications for particle viscosity,  
282 Atmos. Chem. Phys., 18, 2883-2898, <https://doi.org/10.5194/acp-18-2883-2018>, 2018a.
- 283 Huang, Y. L., Zhao, R., Charan, S. M., Kenseth, C. M., Zhang, X., and Seinfeld, J. H.: Unified Theory of Vapor-Wall Mass  
284 Transport in Teflon-Walled Environmental Chambers, Environ. Sci. Technol., 52, 2134-2142,  
285 <https://doi.org/10.1021/acs.est.7b05575>, 2018b.
- 286 Isaacman, G., Kreisberg, N. M., Worton, D. R., Hering, S. V., and Goldstein, A. H.: A versatile and reproducible automatic  
287 injection system for liquid standard introduction: application to in-situ calibration, Atmos. Meas. Tech., 4, 1937-1942,  
288 <https://doi.org/10.5194/amt-4-1937-2011>, 2011.
- 289 Kontogeorgis, G. M., Fredenslund, A., and Tassios, D. P.: Simple Activity-Coefficient Model for The Prediction of Solvent  
290 Activities in Polymer-Solutions, Ind. Eng. Chem. Res., 32, 362-372, <https://doi.org/10.1021/ie00014a013>, 1993.
- 291 Krechmer, J. E., Day, D. A., and Jimenez, J. L.: Always Lost but Never Forgotten: Gas-Phase Wall Losses Are Important in  
292 All Teflon Environmental Chambers, Environ. Sci. Technol., 54, 12890-12897, <https://doi.org/10.1021/acs.est.0c03381>,  
293 2020.
- 294 Krechmer, J. E., Pagonis, D., Ziemann, P. J., and Jimenez, J. L.: Quantification of Gas-Wall Partitioning in Teflon  
295 Environmental Chambers Using Rapid Bursts of Low-Volatility Oxidized Species Generated in Situ, Environ. Sci.  
296 Technol., 50, 5757-5765, <https://doi.org/10.1021/acs.est.6b00606>, 2016.



- 297 Kristensen, K., Jensen, L. N., Glasius, M., and Bilde, M.: The effect of sub-zero temperature on the formation and composition  
298 of secondary organic aerosol from ozonolysis of alpha-pinene, *Environ. Sci.-Process Impacts*, 19, 1220-1234,  
299 <https://doi.org/10.1039/c7em00231a>, 2017.
- 300 Kroll, J. H., Chan, A. W. H., Ng, N. L., Flagan, R. C., and Seinfeld, J. H.: Reactions of semivolatile organics and their effects  
301 on secondary organic aerosol formation, *Environ. Sci. Technol.*, 41, 3545-3550, <https://doi.org/10.1021/es062059x>, 2007.
- 302 Li, Y. T., He, L. K., Xie, D., Zhao, A. Q., Wang, L. X., Kreisberg, N. M., Jayne, J., and Liu, Y. J.: Strong temperature influence  
303 and indiscernible ventilation effect on dynamics of some semivolatile organic compounds in the indoor air of an office,  
304 *Environ. Int.*, 165, <https://doi.org/10.1016/j.envint.2022.107305>, 2022a.
- 305 Li, Y. T., Xie, D., He, L. K., Zhao, A. Q., Wang, L. X., Kreisberg, N. M., Jayne, J., and Liu, Y. J.: Dynamics of di-2-ethylhexyl  
306 phthalate (DEHP) in the indoor air of an office, *Build. Environ.*, 223, <https://doi.org/10.1016/j.buildenv.2022.109446>,  
307 2022b.
- 308 Matsunaga, A. and Ziemann, P. J.: Gas-Wall Partitioning of Organic Compounds in a Teflon Film Chamber and Potential  
309 Effects on Reaction Product and Aerosol Yield Measurements, *Aerosol Sci. Technol.*, 44, 881-892,  
310 <https://doi.org/10.1080/02786826.2010.501044>, 2010.
- 311 McMurry, P. H. and Grosjean, D.: Gas and Aerosol Wall Losses in Teflon Film Smog Chambers, *Environ. Sci. Technol.*, 19,  
312 1176-1182, <https://doi.org/10.1021/es00142a006>, 1985.
- 313 Nakao, S., Shrivastava, M., Anh, N., Jung, H., and Cocker, D., III: Interpretation of Secondary Organic Aerosol Formation  
314 from Diesel Exhaust Photooxidation in an Environmental Chamber, *Aerosol Sci. Technol.*, 45,  
315 <https://doi.org/10.1080/02786826.2011.573510>, 2011.
- 316 Ng, N. L., Chhabra, P. S., Chan, A. W. H., Surratt, J. D., Kroll, J. H., Kwan, A. J., McCabe, D. C., Wennberg, P. O., Sorooshian,  
317 A., Murphy, S. M., Dalleska, N. F., Flagan, R. C., and Seinfeld, J. H.: Effect of NO<sub>x</sub> level on secondary organic aerosol  
318 (SOA) formation from the photooxidation of terpenes, *Atmos. Chem. Phys.*, 7, 5159-5174, [https://doi.org/10.5194/acp-](https://doi.org/10.5194/acp-7-5159-2007)  
319 [7-5159-2007](https://doi.org/10.5194/acp-7-5159-2007), 2007.
- 320 Pratap, V., Bian, Q. J., Kiran, S. A., Hopke, P. K., Pierce, J. R., and Nakao, S.: Investigation of levoglucosan decay in wood  
321 smoke smog-chamber experiments: The importance of aerosol loading, temperature, and vapor wall losses in interpreting  
322 results, *Atmos. Environ.*, 199, 224-232, <https://doi.org/10.1016/j.atmosenv.2018.11.020>, 2019.
- 323 Pratap, V., Kiran, S. A., Bian, Q., Pierce, J. R., Hopke, P. K., and Nakao, S.: Observation of Vapor Wall Deposition in a Smog  
324 Chamber Using Size Evolution of Pure Organic Particles, *Aerosol Air Qual. Res.*, 20, 2705-2714,  
325 <https://doi.org/10.4209/aaqr.2020.05.0268>, 2020.
- 326 Quelever, L. L. J., Kristensen, K., Jensen, L. N., Rosati, B., Teiwes, R., Daellenbach, K. R., Perakyla, O., Roldin, P., Bossi,  
327 R., Pedersen, H. B., Glasius, M., Bilde, M., and Ehn, M.: Effect of temperature on the formation of highly oxygenated  
328 organic molecules (HOMs) from alpha-pinene ozonolysis, *Atmos. Chem. Phys.*, 19, 7609-7625,  
329 <https://doi.org/10.5194/acp-19-7609-2019>, 2019.



- 330 Simon, M., Dada, L., Heinritzi, M., Scholz, W., Stolzenburg, D., Fischer, L., Wagner, A. C., Kurten, A., Rorup, B., He, X. C.,  
331 Almeida, J., Baalbaki, R., Baccharini, A., Bauer, P. S., Beck, L., Bergen, A., Bianchi, F., Brakling, S., Brilke, S., Caudillo,  
332 L., Chen, D. X., Chu, B. W., Dias, A., Draper, D. C., Duplissy, J., El-Haddad, I., Finkenzeller, H., Frege, C., Gonzalez-  
333 Carracedo, L., Gordon, H., Granzin, M., Hakala, J., Hofbauer, V., Hoyle, C. R., Kim, C., Kong, W. M., Lamkaddam, H.,  
334 Lee, C. P., Lehtipalo, K., Leiminger, M., Mai, H. J., Manninen, H. E., Marie, G., Marten, R., Mentler, B., Molteni, U.,  
335 Nichman, L., Nie, W., Ojdanic, A., Onnela, A., Partoll, E., Petaja, T., Pfeifer, J., Philippov, M., Quelever, L. L. J.,  
336 Ranjithkumar, A., Rissanen, M. P., Schallhart, S., Schobesberger, S., Schuchmann, S., Shen, J. L., Sipila, M., Steiner, G.,  
337 Stozhkov, Y., Tauber, C., Tham, Y. J., Tome, A. R., Vazquez-Pufleau, M., Vogel, A. L., Wagner, R., Wang, M. Y., Wang,  
338 D. S., Wang, Y. H., Weber, S. K., Wu, Y. S., Xiao, M., Yan, C., Ye, P. L., Ye, Q., Zauner-Wieczorek, M., Zhou, X. Q.,  
339 Baltensperger, U., Dommen, J., Flagan, R. C., Hansel, A., Kulmala, M., Volkamer, R., Winkler, P. M., Worsnop, D. R.,  
340 Donahue, N. M., Kirkby, J., and Curtius, J.: Molecular understanding of new-particle formation from alpha-pinene  
341 between-50 and+25 degrees C, *Atmos. Chem. Phys.*, 20, 9183-9207, <https://doi.org/10.5194/acp-20-9183-2020>, 2020.
- 342 Song, C., Na, K. S., and Cocker, D. R.: Impact of the hydrocarbon to NO<sub>x</sub> ratio on secondary organic aerosol formation,  
343 *Environ. Sci. Technol.*, 39, 3143-3149, <https://doi.org/10.1021/es0493244>, 2005.
- 344 Voigtlaeander, J., Duplissy, J., Rondo, L., Kuerten, A., and Stratmann, F.: Numerical simulations of mixing conditions and  
345 aerosol dynamics in the CERN CLOUD chamber, *Atmos. Chem. Phys.*, 12, 2205-2214, [https://doi.org/10.5194/acp-12-  
346 2205-2012](https://doi.org/10.5194/acp-12-2205-2012), 2012.
- 347 Wang, M. Y., Xiao, M., Bertozzi, B., Marie, G., Rorup, B., Schulze, B., Bardakov, R., He, X. C., Shen, J. L., Scholz, W.,  
348 Marten, R., Dada, L., Baalbaki, R., Lopez, B., Lamkaddam, H., Manninen, H. E., Amorim, A., Ataci, F., Bogert, P.,  
349 Brasseur, Z., Caudillo, L., De Menezes, L. P., Duplissy, J., Ekman, A. M. L., Finkenzeller, H., Carracedo, L. G., Granzin,  
350 M., Guida, R., Heinritzi, M., Hofbauer, V., Hohler, K., Korhonen, K., Krechmer, J. E., Kurten, A., Lehtipalo, K., Mahfouz,  
351 N. G. A., Makhmutov, V., Massabo, D., Mathot, S., Mauldin, R. L., Mentler, B., Muller, T., Onnela, A., Petaja, T.,  
352 Philippov, M., Piedehierro, A. A., Pozzer, A., Ranjithkumar, A., Schervish, M., Schobesberger, S., Simon, M., Stozhkov,  
353 Y., Tome, A., Umo, N. S., Vogel, F., Wagner, R., Wang, D. S., Weber, S. K., Welti, A., Wu, Y. S., Zauner-Wieczorek,  
354 M., Sipila, M., Winkler, P. M., Hansel, A., Baltensperger, U., Kulmala, M., Flagan, R. C., Curtius, J., Riipinen, I., Gordon,  
355 H., Lelieveld, J., El-Haddad, I., Volkamer, R., Worsnop, D. R., Christoudias, T., Kirkby, J., Mohler, O., and Donahue, N.  
356 M.: Synergistic HNO<sub>3</sub>-H<sub>2</sub>SO<sub>4</sub>-NH<sub>3</sub> upper tropospheric particle formation, *Nature*, 605, 483-+,  
357 <https://doi.org/10.1038/s41586-022-04605-4>, 2022.
- 358 Yeh, G. K. and Ziemann, P. J.: Alkyl Nitrate Formation from the Reactions of C-8-C-14 n-Alkanes with OH Radicals in the  
359 Presence of NO<sub>x</sub>: Measured Yields with Essential Corrections for Gas-Wall Partitioning, *J. Phys. Chem. A*, 118, 8147-  
360 8157, <https://doi.org/10.1021/jp500631v>, 2014.
- 361 Yeh, G. K. and Ziemann, P. J.: Gas-Wall Partitioning of Oxygenated Organic Compounds: Measurements, Structure-Activity  
362 Relationships, and Correlation with Gas Chromatographic Retention Factor, *Aerosol Sci. Technol.*, 49, 726-737,  
363 <https://doi.org/10.1080/02786826.2015.1068427>, 2015.



- 364 Yu, S., Jia, L., Xu, Y., Zhang, H., Zhang, Q., and Pan, Y.: Wall losses of oxygenated volatile organic compounds from  
365 oxidation of toluene: Effects of chamber volume and relative humidity \*, J. Environ. Sci., 114, 475-484,  
366 <https://doi.org/10.1016/j.jes.2021.09.026>, 2022.
- 367 Zhang, X., Cappa, C. D., Jathar, S. H., McVay, R. C., Ensberg, J. J., Kleeman, M. J., and Seinfeld, J. H.: Influence of vapor  
368 wall loss in laboratory chambers on yields of secondary organic aerosol, Proc. Natl. Acad. Sci. U. S. A., 111, 5802-5807,  
369 <https://doi.org/10.1073/pnas.1404727111>, 2014.
- 370 Zhang, X., Schwantes, R. H., McVay, R. C., Lignell, H., Coggon, M. M., Flagan, R. C., and Seinfeld, J. H.: Vapor wall  
371 deposition in Teflon chambers, Atmos. Chem. Phys., 15, 4197-4214, <https://doi.org/10.5194/acp-15-4197-2015>, 2015.
- 372 Zhao, Y. L., Kreisberg, N. M., Worton, D. R., Teng, A. P., Hering, S. V., and Goldstein, A. H.: Development of an In Situ  
373 Thermal Desorption Gas Chromatography Instrument for Quantifying Atmospheric Semi-Volatile Organic Compounds,  
374 Aerosol Sci. Technol., 47, 258-266, <https://doi.org/10.1080/02786826.2012.747673>, 2013.



## 375 Nomenclature

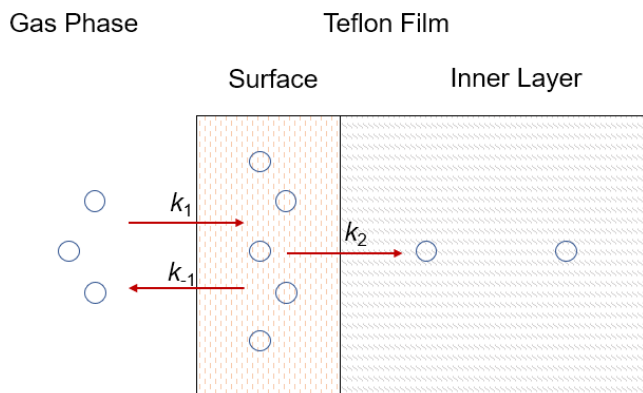
376 A table that contains the definitions of parameters and corresponding units.

|     |                         |   |
|-----|-------------------------|---|
| 377 | $k_1$                   | forward rate constant ( $\text{min}^{-1}$ )   |
| 378 | $k_{-1}$                | backward rate constant ( $\text{min}^{-1}$ )  |
| 379 | $k_2$                   | first-order loss rate constant ( $\text{min}^{-1}$ )                                    |
| 380 | $\tau_{surface}$        | gas-surface equilibrium time scale (min)  |
| 381 | $\tau_{inner}$          | diffusion time scale (min)  |
| 382 | $C_0$                   | initial SVOC concentration in gas phase ( $\mu\text{g m}^{-3}$ )                        |
| 383 | $C_{gas}$               | SVOC concentration in gas phase ( $\mu\text{g m}^{-3}$ )                                |
| 384 | $C_{wall}$              | SVOC concentration on wall surface ( $\mu\text{g m}^{-3}$ )                             |
| 385 | $K_{eq}$                | gas-surface equilibrium constant  |
| 386 | $C_{FEP\_surface}$      | equivalent organic mass concentration of the FEP chamber surface ( $\text{mg m}^{-3}$ ) |
| 387 | $M_{wall}$              | average molecular mass of the Teflon wall ( $\text{g mol}^{-1}$ )                       |
| 388 | $\gamma_{FEP\_surface}$ | activity coefficient in the Teflon surface  |
| 389 | $R$                     | gas constant ( $\text{J K}^{-1} \text{mol}^{-1}$ )                                      |
| 390 | $T$                     | temperature (K)   |
| 391 | $P_s(T)$                | saturation vapor pressure of compound at temperature $T$ (Pa)                           |



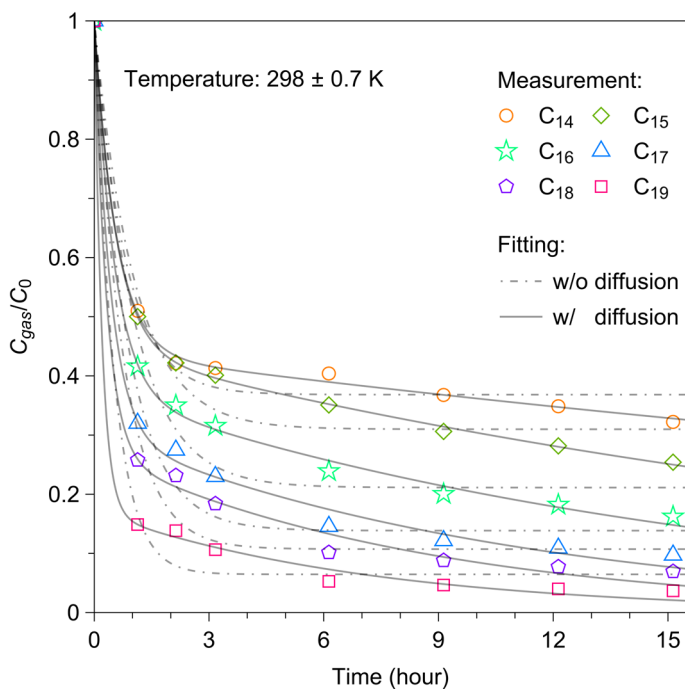
392

393 **Figure 1.** Schematic diagram of the experimental setup.



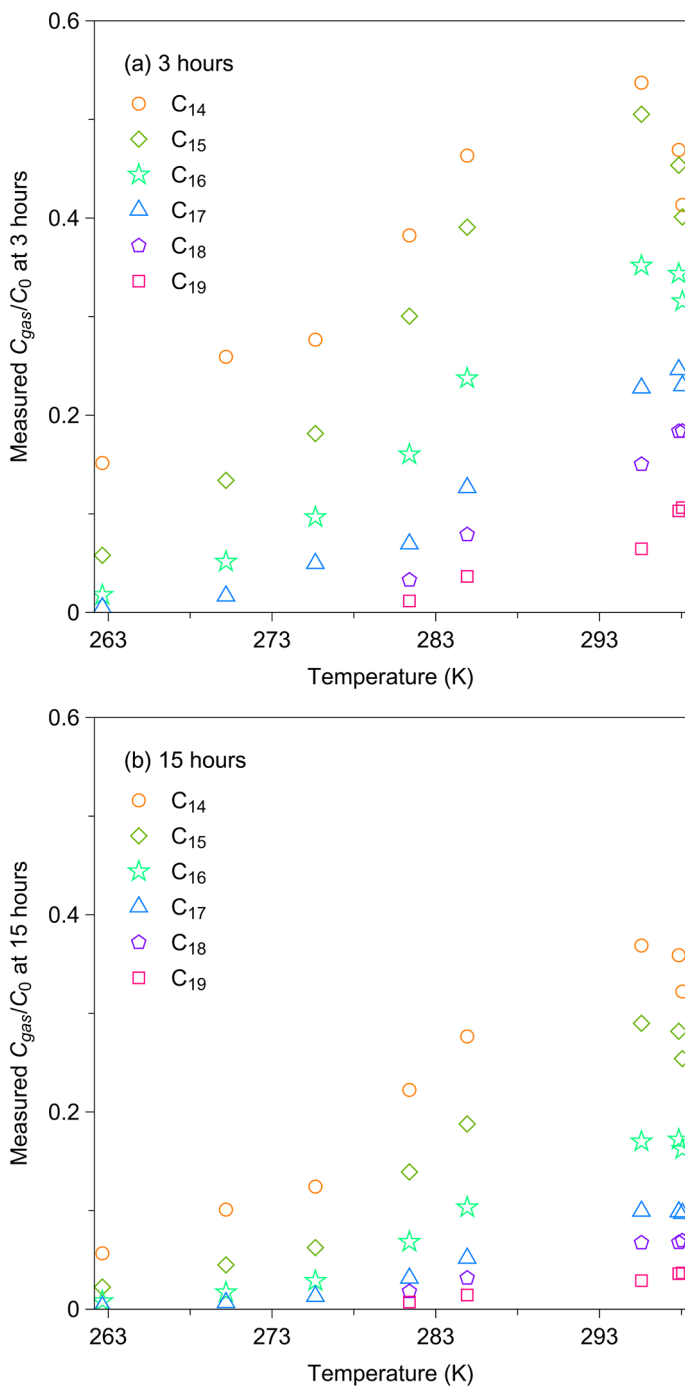
394

395 **Figure 2.** Schematic diagram of wall loss process. Compounds partition between gas phase and surface layer with forward  
396 and backward rates ( $k_1$  and  $k_{-1}$ ). Compounds in surface layer undergo irreversible diffusion into inner layer with first-order  
397 loss rate ( $k_2$ ).



398

399 **Figure 3.** Temporal variation in  $C_{gas}/C_0$  for C<sub>14</sub>-C<sub>19</sub> *n*-alkanes at  $298 \pm 0.7$  K following injection.  $C_{gas}$  is the concentration of  
400 each *n*-alkane in the gas phase, and  $C_0$  is the corresponding initial concentration of each *n*-alkane. The two-layer kinetic  
401 sorption model (Section 2.2) was employed to fit the data (black solid line). The black dot-dashed lines show the fitting result  
402 to the model that ignores the diffusion process to the inner layer (*i.e.*,  $k_2 = 0$ ).



403

404 **Figure 4.** Measured values of  $C_{gas}/C_0$  at (a) 3 hours and (b) 15 hours after injection.

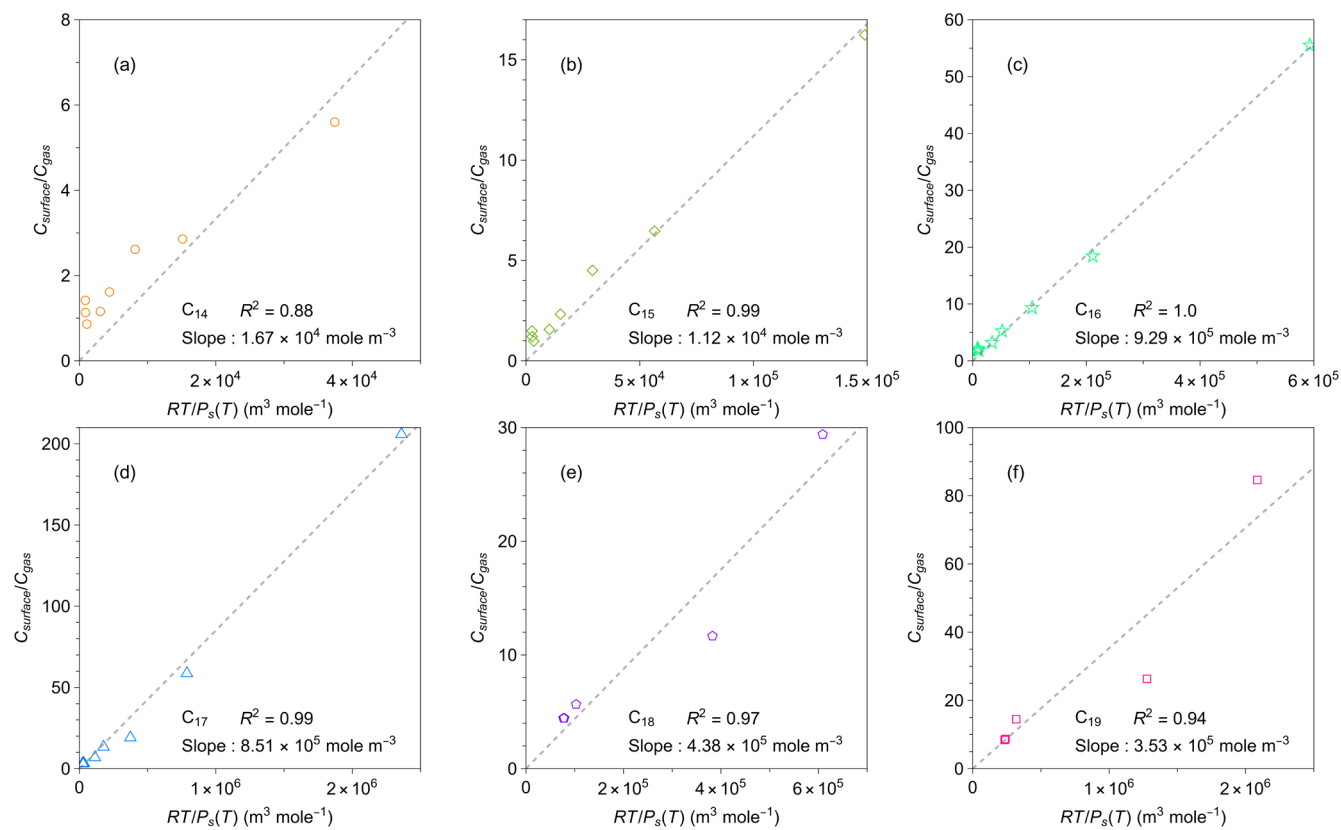
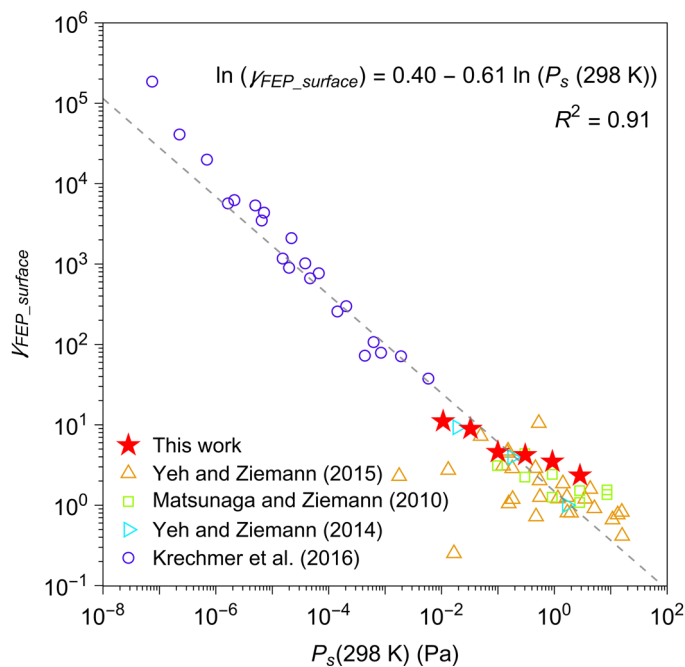
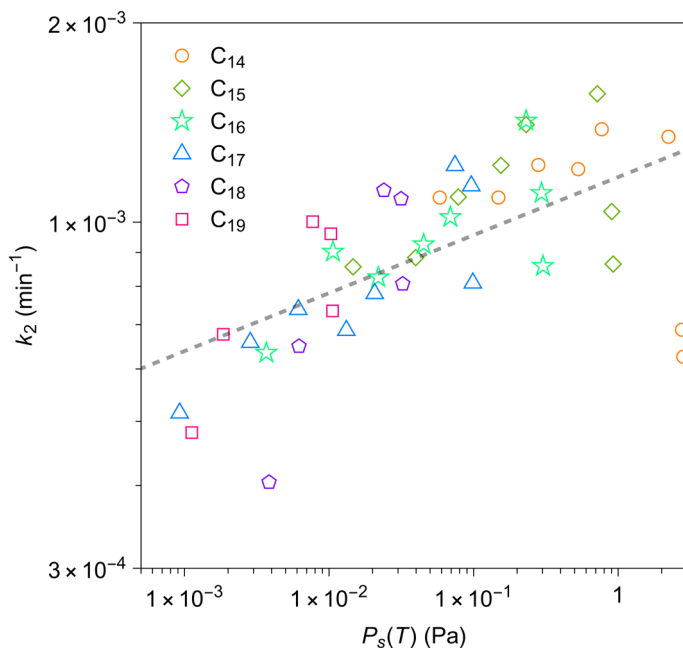


**Figure 5.** Relationships between measured ratio of concentrations in the chamber wall surface phase and in the gas phase at quasi-equilibrium and calculated values of  $RT/P_s(T)$  for individual  $n$ -alkanes. Calculation methods for  $C_{surface}/C_{gas}$  is detailed in the text. The values of  $RT/P_s(T)$  for each  $n$ -alkane were calculated by the EVAPORATION group contribution method (Compernelle et al., 2011). The black dashed lines are linear least-squares that fit the data for each  $n$ -alkane.



411 **Figure 6.** Activity coefficient ( $\gamma_{FEP\_surface}$ ) of organic compounds in FEP film. The sources of data include this work and the  
412 literature (Matsunaga and Ziemann, 2010; Yeh and Ziemann, 2014; Yeh and Ziemann, 2015; Krechmer et al., 2016). A list of  
413 chemical species that were investigated by each study is available in Table S4. Saturation vapor pressures at 298 K ( $P_s(298\text{ K})$ )  
414 were estimated by EVAPORATION (Compernelle et al., 2011).



415

416 **Figure 7.** Relationship between calculated first-order loss rate  $k_2$  for each  $n$ -alkane and calculated values of saturation vapor  
417 pressure by the EVAPORATION group contribution method (Compernelle et al., 2011). The calculation method for  $k_2$  is  
418 detailed in the text. The black dashed line is a linear least-squares fit to the data in a logarithmic scale.